Journal of *Xenobiotics*

MDPI

Article

Enzyme-Targeted Antiproliferative Effects of Novel Indole–Acrylamide Xenobiotics Acting on Cyclooxygenase Pathways

Mohammed Hawash [1,*], Benay Mahmutoğlu [2], Murad Abualhasan [1], Deniz Cansen Kahraman [3] and Sultan Nacak Baytas [2,*]

[1] Department of Pharmaceutical Chemistry and Technology, Faculty of Pharmacy, An-Najah National University, Nablus 00433, Palestine; m_abualhasan@najah.edu
[2] Department of Pharmaceutical Chemistry, Faculty of Pharmacy, Gazi University, Ankara 06330, Turkey; benaymahmutoglu@hotmail.com
[3] Cancer Systems Biology Laboratory, Department of Health Informatics, Graduate School of Informatics, Middle East Technical University, Ankara 06800, Turkey; denizcansen89@gmail.com
* Correspondence: mohawash@najah.edu (M.H.); baytas@gazi.edu.tr (S.N.B.); Tel.: +970-2569939939 (M.H.); +90-312-202-3225 (S.N.B.)

Abstract

The indole scaffold is common in natural products and bioactive compounds, including anti-cancer and anti-inflammatory medicines. In this work, a series of indole-acrylamide derivatives was synthesized, and their antiproliferative and anti-inflammatory effects were evaluated on COX enzymes and against a panel of cancer cell lines. All the final compounds were characterized via HRMS and (^{1}H & ^{13}C)-NMR. Anticancer and anti-inflammatory activities were evaluated using standard biomedical techniques by SRB, MTS, and COX kit assays. Additionally, the molecular docking analysis was conducted using the AutoDock Vina tool. The results demonstrated that the produced compounds displayed significant inhibitory effects on the COX-2 enzyme, with IC_{50} values of 128 nM to 1.04 μM. **6a** demonstrated significant COX-2 selectivity with an IC_{50} of 128 nM and an SI of 352, highlighting its preference for COX-2 over COX-1. **6c** exhibited potent COX-2 inhibition with an IC_{50} of 0.215 μM and an SI of 10.6. The assessed compounds exhibited substantial cytotoxic effects on cancer cells, especially against liver cancer cell lines (Huh7, HepG2, Mahlavu, and SNU475), and breast cancer (MCF-7). **6d** compound was the most COX-1 selective inhibitor, which observed potent activity against hepatocellular carcinoma, with IC_{50} values as low as 3.5 μM, and was highly effective against MCF-7. Additionally, COX-2 selective inhibitors, **6a** and **6b**, exhibited strong antiproliferative effects against both breast cancer (MCF-7) and melanoma (B16F1), with IC_{50} values ranging from 4.75 to 15.4 μM. Furthermore, the molecular docking of **6a** demonstrated a strong affinity for the COX-2 enzyme, with energy scores (S) of −8.392 kcal/mol, comparable to celecoxib's score of −10.96 kcal/mol. The findings suggest a possible correlation between COX-2 inhibition and anticancer efficacy, especially for compounds **6a** and **6c**, which demonstrate excellent COX-2 selectivity and notable antiproliferative effects, positioning them as prospective candidates for further advancement in cancer treatment.

Keywords: indole; COX; cancer; selectivity; cell lines; molecular docking

Academic Editors: Weimin Gao and Andrei Flavius Radu

Received: 20 January 2026
Revised: 22 February 2026
Accepted: 28 February 2026
Published: 4 March 2026

1. Introduction

COX-1 and COX-2 enzymes facilitate the pivotal stage of prostaglandin production. Given their role in tumor progression, these isoforms have emerged as vital targets for contemporary cancer pharmacology [1]. Although expressed differently, both COX-1 and COX-2 are associated with inflammatory reactions and overexpressed in many malignancies [2]. Multiple malignancies have been linked to COX-2, which contributes to carcinogenesis and cancer cell resistance to radiotherapy and chemotherapy [3]. Solid tumors, including breast and bladder cancer, have elevated COX-2 levels [4,5]. COX-2 overexpression is also found in colorectal, pancreatic, and lung tumors [6,7]. COX-2 inhibits apoptosis, stimulates epidermal growth factor receptors, activates the mitogen-activated protein kinase cascade, and binds to tyrosine. COX-2 may also break matrix metalloproteinase, causing cell membrane rupture, metastasis, and tumor invasiveness [8,9].

Recent comprehensive analyses have further elucidated that the pro-tumorigenic role of COX-2 extends beyond simple inflammation; it is a master regulator of the tumor microenvironment, affecting angiogenesis and the maintenance of cancer stem cell (CSC) populations [10]. The accumulation of COX-2 metabolites supports a multifaceted array of oncogenic processes, including metabolic transformation and the evasion of apoptosis, which collectively facilitate tumor survival and metastatic dissemination. Consequently, targeting the COX-2 pathway—via both dependent and independent mechanisms—remains a cornerstone of modern chemoprotective strategies and justifies the rational design of novel inhibitors as potential anticancer candidates [10,11].

Inflammation and malignancy increase COX-2 levels [12], making COX-2 inhibitors promising antiproliferative agents [13,14]. In human and animal models of colon cancer, NSAIDs, including non-selective inhibitors like aspirin, reduce colon cancer risk and promote tumor regression [15,16].

In medicinal chemistry, indole is a significant structural framework. Considerable pharmacological effects have been documented in indole derivatives. Indole derivatives have been employed as anti-inflammatory, analgesic, antipyretic [17], and anticancer therapeutics [18]. Strong anticancer alkaloids such as the vincristine family include the indole scaffold [19]. Concurrently, it was shown that indomethacin (Figure 1), a COX-1 and COX-2 inhibitor derived from indole, displayed anti-lung cancer and anti-CRC properties by chemical alterations in its primary structure [20].

In particular, the COX-2 inhibitor celecoxib (Figure 1) has shown significant anticancer properties in specific cancer forms such as ovarian cancer and adenomas [21]. In male F344 rats, the selective COX-1 inhibitor mofezolac (Figure 1) has been shown to suppress the growth of colon cancers produced by azoxymethane. This inhibition is supported by evaluations of tumor incidence, multiplicity, and volume [22].

Penthala et al. synthesized a series of novel indol-thioxodihydropyrimidine derivatives and evaluated them for their antiproliferative activities against various cancer cell lines. Among this series, St.1 (Figure 1) showed significant growth inhibition against melanoma cancer cell lines (MDA-MB-435) with a GI_{50} value of 0.85 μM. In the docking studies, this compound was well bound to the COX-2 binding pocket via strong hydrogen and hydrophobic bonds [23]. For instance, St.2 (Figure 1) showed significant inhibition of the COX-2 enzyme (61%) at a concentration of 25 μM. This inhibition was found to be correlated with anticancer activity, as indicated by an IC_{50} value of 0.67 μM against MCF-7 cancer cell lines [24]. In our last works regarding the indole derivatives, a lot of indole derivatives showed significant anticancer activities, especially those with the tert-butylphenyl moiety St.3 (Figure 1), and the linkers were isoxazole, pyrazole, alkene, and substituted alkene [18,25,26]. Additionally, in our last works, we have synthesized a series of structures that contain isoxazole-carboxamide, and notably, the compounds contain-

ing a tert-butylphenyl moiety displayed dual effects on COX-2 enzyme IC_{50} 3.22 μg/mL and IC_{50} 2.77, 18.22, and 9.31 μg/mL against Hep3B, HeLa, and MCF-7, respectively [27]. In contrast, St.5 exhibited significant inhibitory effects on COX, measured by IC_{50} values of 0.239 and 0.191 μM against COX-1 and COX-2, respectively. Nevertheless, it displayed little effectiveness in combating COLO205 cancer cell lines, with an IC_{50} value of 30.79 μM [28].

The rationale behind the design of these novel indole–acrylamide hybrids from the indole scaffold status and the strategic incorporation of the acrylamide linker. While the indole core provides a robust framework for COX-binding affinity—mimicking traditional NSAIDs like indomethacin—the acrylamide moiety was specifically selected to serve as a rigid spacer to enhance interactions within the hydrophobic pockets of the COX-2 enzyme. Although these compounds exhibit clear anti-inflammatory potential through COX inhibition, they are not categorized solely as traditional anti-inflammatory agents due to their dual-functional design. The structural modifications were engineered to transcend simple prostaglandin suppression. In the course of our investigation, the hybridization strategy was conducted to connect the indole and tert-butylphenyl moieties in the same structures; these structures were designed to demonstrate anticancer and COX inhibition activities. This study seeks to create a new series of tert-butyl-phenyl-indol-methylacrylamide derivatives and evaluate their effects on COX enzymes and their cytotoxicity in various cancer and normal cell lines, expanding on prior findings. This method functions as a strong strategy to further confirm the efficacy of our medicines as COX inhibitors. Molecular docking analyses are set to provide a comprehensive knowledge of the binding interactions between our drugs and the COX-2 enzyme, clarifying the rationale for their observed COX inhibitory effect.

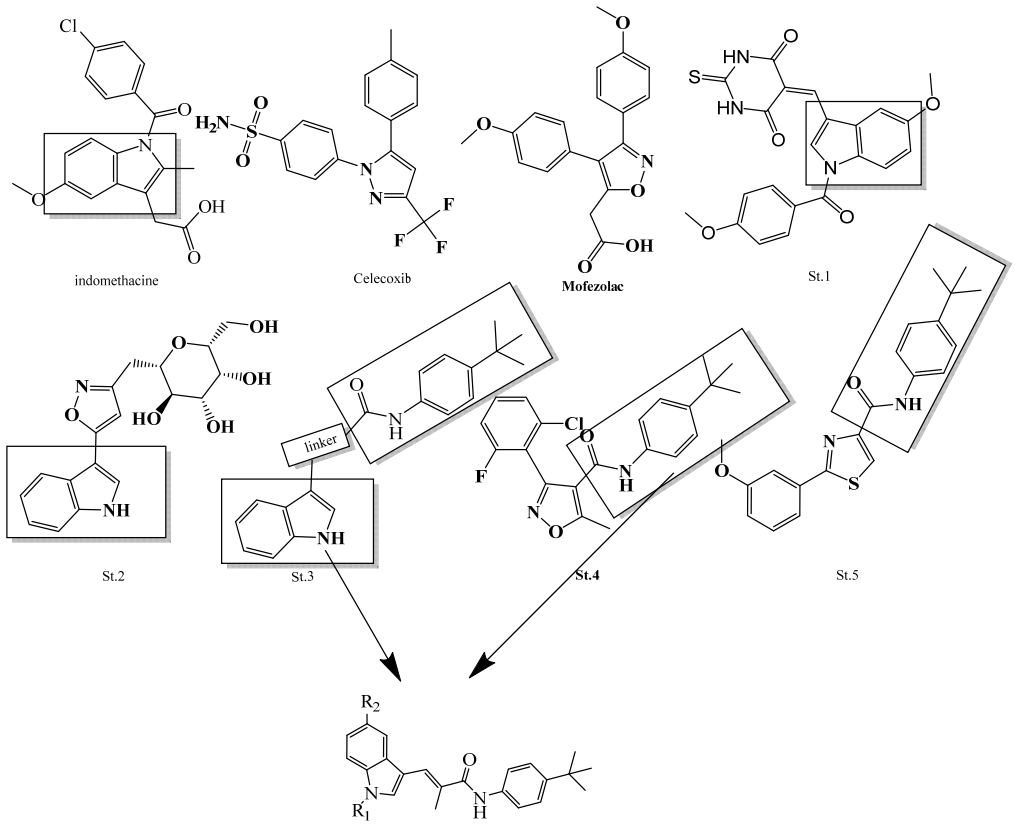

Figure 1. The chemical structures of the compounds exhibit dual functionality as COX inhibitors and possess anticancer properties.

2. Materials and Methods

2.1. Chemistry

Commercial reagents and solvents were used, with normal solvent drying methods where needed. The SMP-II Digital Melting Point Apparatus (Schorpp Geaetetechnik, Überlingen, Germany) was used for all final compound melting points (M.P.) without correction. The Faculty of Pharmacy, Ankara University, analyzed the produced compounds' ^{1}H and ^{13}C NMR spectra in DMSO-d6 solutions using a Bruker DPX-400 High-Performance Digital FT-NMR Spectrometer (Billerica, MA, USA). The ^{1}H-NMR spectra were taken at 400 MHz and the ^{13}C-spectra at 101 MHz. Chemical shift values (δ) were measured in ppm, while coupling constants were in Hz. The water LCT Premier XE Mass Spectrometer (Waters Corporation, Milford, MA, USA) was used to collect high-resolution mass spectra (HRMS) data using positive polarity electrospray ionization (ESI).

2.1.1. General Procedure of (E)-Ethyl 3-(1H-Indol-3-yl)-2-methylacrylate Derivatives (**2**,**3**)

Into the solution of compound **1** (0.5 g, 3.44 mmol) in anhydrous DMF (5 mL), sodium hydride (440 mmol) was added at room temperature; 10 min later, the appropriate benzyl bromide or methyl iodide (3.9 mmol) was added, and the mixture was stirred for 20 min. The mixture was then poured into a cold NaCl-saturated solution. The precipitate was collected by vacuum filtration and washed with distilled water, dried in a vacuum oven. After that, each derivative of indole aldehyde (1 eq) and (carbethoxyethylidene) triphenylphosphorane (1.3 eq) was dissolved in DCM. The reaction solution was refluxed for 18 h, and the excess solvent was evaporated under reduced pressure. The residue was purified by column flash chromatography on silica gel using n-Hexane: EtOA (1:1) to give the desired products **2**, **3**.

(E)-Ethyl 2-Methyl-3-(1-methyl-1H-indol-3-yl)acrylate (**2a**)

Solid product, M.P. 120–122 °C. Yield 45%. IR (FTIR/FTNIR-ATR) cm^{-1}: 2987-2908 (C-H aliphatic), 1673 (C=O). HRMS (ESI): *m*/*z* calcd. for $C_{15}H_{18}NO_2$ $[M+H]^+$:244.1338; found: 244.1327. ^{1}H NMR (DMSO-d_6) δ: 7.91 (1H, d, indole H-2), 7.81 (1H, s, β-H), 7.72 (1H, d, *J* = 8 Hz, indole H-4), 7.50 (1H, d, *J* = 8 Hz, indole H-7), 7.25 (1H, td, *J* = 7.2, 1 Hz indole H-5), 7.17 (1H, td, *J* = 7.4, 0.8 Hz indole H-6), 4.18 (2H, q, *J* = 7.2 Hz, O-**CH$_2$**-), 3.86 (3H, s, N-methyl), 3.10 (3H, s, methyl),1.28 (3H, t, *J* = 6.8 Hz, O-CH$_2$-**CH$_3$**). ^{13}C NMR (DMSO-d_6) δ: 167.99, 136.18, 131.63, 129.42, 127.70, 122.35, 120.62, 120.34, 118.03, 110.24, 110.13, 60.00, 32.89, 14.86, 14.29.

(E)-Ethyl 3-(5-Bromo-1-methyl-1H-indol-3-yl)-2-methylacrylate (**2b**)

Solid product, M.P. 113–113.5 °C. Yield 57%. IR (FTIR/FTNIR-ATR) cm^{-1}: 2965-2856 (C-H aliphatic), 1647 (C=O). HRMS (ESI): *m*/*z* calcd. for $C_{15}H_{17}NO_2Br$ $[M+H]^+$: 322.0443; found: 322.0430. ^{1}H NMR ($DMSO_6$) δ: 7.91 (1H, d, *J* = 2 Hz, indole H-2), 7.85 (1H, s, β-H), 7.82 (1H, s, indole H-4), 7.49 (1H, d, *J* = 8.8 Hz, indole H-7), 7.36 (1H, dd, *J* = 8.8, 2 Hz indole H-6), 4.18 (2H, q, *J* = 6.8 Hz, O-**CH$_2$**-), 3.86 (3H, s, N-methyl), 2.09 (3H, d, *J* = 1.2 Hz, methyl), 1.28 (3H, t, *J* = 6.8 Hz, O-CH$_2$-**CH$_3$**). ^{13}C NMR ($DMSO_6$) δ: 167.88, 134.95, 132.84, 129.36, 128.77, 124.84, 121.54, 120.52, 113.15, 112.43, 109.76, 60.08, 33.09, 14.87, 14.28.

(E)-Ethyl 3-(1-Benzyl-5-bromo-1H-indol-3-yl)-2-methylacrylate (**3b**)

Solid product, M.P. 111–112 °C. Yield 79%. IR (FTIR/FTNIR-ATR) cm^{-1}: 2964-2866 (C-H aliphatic), 1634 (C=O). HRMS (ESI): *m*/*z* calcd. for $C_{21}H_{21}NO_2Br$ $[M+H]^+$: 398.0756; found: 398.0757. ^{1}H NMR (DMSO-d6) δ: 8.10 (1H, s, indole H-2), 7.93 (1H, d, *J* = 2 Hz, β-H), 7.86 (1H, s, indole H-4), 7.49 (1H, d, *J* = 8.8 Hz, indole H-6), 7.34-7.24 (6H, m, indole H-7, phenyl-H), 5.53 (2H, s, phenyl-**CH$_2$**), 4.21 (2H, q, *J* = 7.2 Hz, O-**CH$_2$**-), 2.13 (3H, d,

J = 1.2 Hz, methyl), 1.30 (3H, t, J = 6.8 Hz, O-CH_2-**CH_3**). ^{13}C NMR (DMSO-d_6) δ: 167.83, 137.21, 134.22, 132.29, 129.71, 128.67, 128.61, 127.58, 127.04, 125.04, 122.21, 120.77, 113.30,112.89, 110.34, 60.12, 49.62, 14.97, 14.27.

2.1.2. General Synthetic Procedure for Hydrolysis (E)-2-Methyl-3-(1H-indol-3-yl)acrylic Acid (**4**, **5**)

Acrylate (1 eq) was dissolved in a mixture of methanol, water, and THF solvent, and Lithium hydroxide (10 equiv.) at 5 °C. The solution was refluxed for 3 h before it was cooled to room temperature. The solution was then evaporated, and the residue was made acidic (pH = 2) by the addition of HCl. The precipitate was filtered and concentrated in a vacuum to give the crude products 4, 5, which were used without further purification.

(E)-2-Methyl-3-(1-methyl-1H-indol-3-yl)acrylic Acid (**4a**)

Solid product, M.P. 199–201 °C. Yield 99%. IR (FTIR/FTNIR-ATR) cm^{-1}: 2988-2920 (C-H aliphatic), 3221-2300 (O-H), 1655 (C=O). HRMS (ESI): m/z calcd. for $C_{13}H_{14}NO_2$ $[M+H]^+$: 216.1025; found: 216.1013. ^{1}H NMR (DMSO-d_6) δ: 12.06 (1H, s, O-H), 7.89 (1H, d, indole H-2), 7.78 (1H, s, β-H), 7.71 (1H, d, J = 7.6 Hz, indole H-4), 7.49 (1H, d, J = 8.4 Hz, indole H-7), 7.25 (1H, td, J = 7.4, 1.2 Hz indole H-5), 7.16 (1H, td, J = 7.6, 0.8 Hz indole H-6), 3.86 (3H, s, N-C**H_3**), 2.08 (3H, d, J = 0.8 Hz, methyl). ^{13}C NMR (DMSO-d_6) δ: 169.69, 136.17, 131.39, 129.06, 127.72, 122.30, 121.36, 120.27, 118.06, 110.32, 110.20, 32.87, 14.87.

(E)-3-(5-Bromo-1-methyl-1H-indol-3-yl)-2-methylacrylic Acid (**4b**)

Solid product, M.P. 254–255 °C. Yield 88%. IR (FTIR/FTNIR-ATR) cm^{-1}: 3288-2351 (O-H), 2963-2866 (C-H aliphatic), 1634 (C=O). HRMS (ESI): m/z calcd. for $C_{13}H_{13}NO_2Br$ $[M+H]^+$: 294.0130; found: 294.0133. ^{1}H NMR (DMSO-d_6) δ: 12.11 (1H, s, O-H), 7.88 (1H, d, J = 2 Hz, β-H), 7.83 (1H, s, indole H-2), 7.80 (1H, s, indole H-4), 7.48 (1H, d, J = 8.8 Hz, indole H-7), 7.35 (1H, dd, J = 8.6, 1.8 Hz, indole H-6), 3.86 (3H, s, N-**CH_3**), 2.06 (3H, d, J = 0.8 Hz methyl). ^{13}C NMR (DMSO-d_6) δ: 169.57, 134.94, 132.61, 129.39, 128.38, 124.77, 122.30, 120.54, 113.07, 112.38, 109.94, 33.08, 14.86.

(E)-3-(1-Benzyl-1H-indol-3-yl)-2-methylacrylic Acid (**5a**)

Solid product, M.P. 209–211 °C. Yield 98%. HRMS (ESI): m/z calcd. for $C_{19}H_{18}NO_2$ $[M+H]^+$: 292.1338; found: 292.1337. ^{1}H NMR (DMSO-d_6) δ: 12.11 (1H, s, O-H), 8.00 (1H, s, indole H-2), 7.90 (1H, s, β-H), 7.72 (1H, d, J = 7.2 Hz, indole H-4), 7.49 (1H, d, J = 8 Hz, indole H-7), 7.32-7.12 (7H, m, indole H-5, H-6, phenyl-H), 5.51 (2H, s, phenyl-**CH_2-**), 2.10 (3H, d, J = 0.8 Hz, methyl). ^{13}C NMR (DMSO-d_6) δ: 169.64, 137.58, 135.46, 130.86, 128.92, 128.58, 128.03, 127.49, 127.10, 122.44, 122.03, 120.41, 118.27, 110.88, 110.73, 49.48, 14.97.

(E)-3-(1-Benzyl-5-bromo-1H-indol-3-yl)-2-methylacrylic Acid (**5b**)

Solid product, M.P. 236–238 °C. Yield 95%. IR (FTIR/FTNIR-ATR) cm^{-1}: 2965-2951 (C-H aliphatic), 3202-2442 (O-H), 1634 (C=O). HRMS (ESI): m/z calcd. for $C_{19}H_{17}NO_2Br$ $[M+H]^+$: 370.0443; found: 370.0445. ^{1}H NMR (DMSO-d_6) δ: 12.16 (1H, s, O-H), 8.05 (1H, s, indole H-2), 7.89 (1H, d, J = 1.6 Hz, β-H), 7.83 (1H, s, indole H-4), 7.47 (1H, d, J = 8.8 Hz, indole H-6), 7.32-7.23 (6H, m, indole H-7, phenyl-H), 5.51 (2H, s, phenyl-**CH_2-**), 2.09 (3H, s, methyl). ^{13}C NMR (DMSO-d_6) δ: 169.52, 137.27, 134.21, 132.06, 129.74, 128.62, 128.26, 127.58, 127.04, 124.98, 122.95, 120.79, 113.21, 112.85, 110.53, 49.61, 14.97.

2.1.3. General Synthetic Procedure for Indole-Acrylamide Derivatives (**6a–6d**)

The synthesis procedure commenced with the dissolution of each acrylic acid (**4**, **5**) (1 eq) in 20 mL of DCM. Subsequently, DMAP (0.3 eq) and EDC (1.3 eq) were added to the solution, then stirred under inert gas at R.T. for 30 min. 4-tert-butylaniline (1.1 eq) was

then added to the mixture. Afterward, the solvent was eliminated under vacuum pressure, and the residue was re-dissolved in DCM. Final product isolation involved purification through flash chromatography utilizing a suitable solvent system, n-hexane: ethyl acetate (1:1) [18].

(E)-N-(4-(Tert-butyl)phenyl)-2-methyl-3-(1-methyl-1H-indol-3-yl)acrylamide (**6a**)

Solid product, M.P. 70–71 °C. Yield 74%. IR (FTIR/FTNIR-ATR): 3280 (N-H), 2957-2866 (C-H aliphatic), 1635 (C=O). HRMS (ESI): *m*/*z* calcd. for $C_{23}H_{27}N_2O$ $[M+H]^+$: 347.2123; found: 347.2116. ^{1}H NMR (DMSO-d_6) δ: 9.79 (1H, s, N-H), 7.85 (1H, d, *J* = 7.6 Hz, indole H-4), 7.75 (1H, indole H-2), 7.65-7.63 (3H, m, β-H, phenyl H-2, H-6), 7.49 (1H, d, *J* = 8 Hz, indole H-7), 7.33 (2H, d, *J* = 8.4 Hz, phenyl H-3, H-5), 7.27-7.15 (2H, m, indole H-5, H-6), 3.88 (3H, s, N-methyl), 2.89 (3H, s, methyl), 1.27 (9H, s, tert-butyl). ^{13}C NMR (DMSO-d_6) δ: 168.07, 145.26, 137.12, 136.10, 130.50, 127.81, 126.22, 125.00, 124.64, 122.14, 119.99, 119.77, 118.65, 110.49, 110.03, 33.96, 32.81, 31.22, 15.60.

(E)-3-(5-Bromo-1-methyl-1H-indol-3-yl)-N-(4-(tert-butyl)phenyl)-2-methylacrylamide (**6b**)

Solid product, M.P. 79–81 °C. Yield 93%. IR (FTIR/FTNIR-ATR): 3281 (N-H), 2965-2855 (C-H aliphatic), 1635 (C=O). HRMS (ESI): *m*/*z* calcd. for $C_{23}H_{26}N_2OBr$ $[M+H]^+$: 425.1228; found: 425.1224. ^{1}H NMR (DMSO-d_6) δ: 9.77 (1H, s, N-H),8.08 (1H, d, *J* = 1.6 Hz, β-H), 7.79 (1H, s, indole H-2), 7.63 (2H, d, *J* = 8.4 Hz, phenyl H-2, H-6), 7.60 (1H, s, indole H-4), 7.48 (1H, d, *J* = 8.8 Hz, indole H-7), 7.36-7.32 (3H, m, phenyl H-3, H-5, indole H-6), 3.87 (3H, s, N-**CH_3**), 2.14 (3H, s, methyl), 1.27 (9H, s, tert-butyl). ^{13}C NMR (DMSO-d_6) δ: 167.88, 145.34, 137.00, 134.85, 131.74, 129.55, 127.00, 125.00, 124.59, 123.78, 121.13, 120.10, 112.67, 112.22, 110.20, 33.97, 33.01, 31.21, 15.51.

(E)-3-(1-Benzyl-1H-indol-3-yl)-N-(4-(tert-butyl)phenyl)-2-methylacrylamide (**6c**)

Solid product, M.P. 174–175.5 °C. Yield 97%. IR (FTIR/FTNIR-ATR): 3281 (N-H), 2965-2855 (C-H aliphatic), 1635 (C=O). HRMS (ESI): *m*/*z* calcd. for $C_{29}H_{31}N_2O$ $[M+H]^+$: 423.2436; found: 423.2426. ^{1}H NMR (DMSO-d_6) δ: 9.80 (1H, s, N-H), 7.95 (1H, s, indole H-2), 7.85 (1H, d, *J* = 7.2 Hz, indole H-4) 7.65-7.63 (3H, m, β-H, phenyl H-2, H-6), 7.48 (1H, d, *J* = 8 Hz, indole H-7), 7.34-7.22 (7H, m, phenyl-H), 7.20-7.12 (2H, m, indole H-6, H-5), 5.52 (2H, s, phenyl-**CH_2**), 2.18 (3H, s, methyl), 1.27 (9H, s, tert-butyl). ^{13}C NMR (DMSO-d_6) δ: 168.08, 145.30, 137.76, 137.09, 135.42, 130.00, 128.55, 128.10, 127.42, 127.01, 126.91, 125.01, 124.48, 122.29, 119.96, 119.93, 118.84, 111.06, 110.55, 49.39, 33.96, 31.21, 15.69.

(E)-3-(1-Benzyl-5-bromo-1H-indol-3-yl)-N-(4-(tert-butyl)phenyl)-2-methylacrylamide (**6d**)

Solid product, M.P. 199–201 °C. Yield 35%. IR (FTIR/FTNIR-ATR): 3289 (N-H), 2967-2866 (C-H aliphatic), 1634 (C=O). HRMS (ESI): *m*/*z* calcd. for $C_{29}H_{30}N_2OBr$ $[M+H]^+$: 501.1541; found: 501.1561. ^{1}H NMR (DMSO-d_6) δ: 9.82 (1H, s, N-H), 8.11 (1H, s, indole H-2), 8.03 (1H, s, β-H), 7.66-7.27 (12H, s, indole H-4, H-6, H-7, phenyl-H), 5.54 (2H, s, phenyl-**CH_2**), 2.17 (3H, s, methyl), 1.29 (9H, s, tert-butyl). ^{13}C NMR (DMSO-d_6) δ: 167.88, 145.38, 137.43, 136.97, 134.15, 131.22, 129.89, 128.61, 127.68, 127.52, 126.99, 125.02, 124.79, 123.63, 121.35, 120.08, 112.83, 112.69, 110.77, 49.53, 33.89, 31.21, 15.62.

2.2. Biological Assays

2.2.1. COX Assay Method

Cayman Chemical, Ann Arbor, MI, USA, supplied the enzyme immunoassay (EIA) kit 560131 for the in vitro cyclooxygenase inhibition assay. This kit was used to evaluate the inhibitory potential of synthesized indol-acrylamide derivatives (**6a–6d**) and celecoxib

against ovine and human COX-1 and COX-2, respectively, at 0.01, 0.5, 10, and 30 μM concentrations. IC_{50} values were measured in micromoles (μM) using non-linear regression analysis of the log(inhibitor) vs. response curve (four-parameter logistic equation), a previously documented procedure [29].

2.2.2. Cell Culture

The anticancer effects of all final compounds **6a–6d** were tested in vitro against eleven cancer cell lines, including human HCC cell lines (Huh7:JCRB0403, Hep3B: ATCC-HB-8064, HepG2: ATCC-HB-8065), Mahlavu [30] and SNU475: ATCC-CRL-2236), colon cancer cell lines (HCT116: ATCC-CCL-247) and MCF-7: ATCC HTB-22), adenocarcinoma (HeLa: CCL2) and CaCo-2: CRL-2102), normal human embryo kidney (HEK 293T: CRL-3519), and mouse melanoma (B16-F1: CRL-6323). All cell lines were grown in RPMI-1640 media with 10.0% fetal bovine serum, 1.0% l-glutamine, and 1.0% Penicillin/Streptomycin antibiotics at 37 °C in a humid environment with 5.0% CO_2 [31]. All cell lines are registered in the Cellosaurus database and were obtained from the American Type Culture Collection (ATCC, Manassas, VI, USA) or the Japanese Collection of Research Bioresources (Osaka, Japan).

Cells were seeded in 96-well plates at a density of 2.5×10^4 cells per well. After 24 h to allow attachment, the culture medium was replaced, and cells were treated with compounds **6a–6d** at five concentrations (1, 10, 50, 100, and 300 μM) for 24 h to determine IC_{50} values. Cell viability was assessed using the CellTiter 96® Aqueous One Solution Cell Proliferation (MTS) (Promega Corporation, Madison, WI, USA) assay according to the manufacturer's instructions. Briefly, 20 μL of MTS reagent was added to each well containing 100 μL of culture medium and incubated at 37 °C for 2 h. Absorbance was measured at 490 nm using a microplate reader [32].

Huh7, HepG2, Mahlavu, SNU475, MCF7, and HCT116 cells were seeded at $2–3 \times 10^4$ cells/well into Corning® 96-well plates (354516) for 24h before treatment. The test compounds and sorafenib (positive control, Selleckchem S7397) were dissolved in DMSO (Sigma-Aldrich, cat. no. D2650; Burlington, MA, USA). Cells were treated with five concentrations ranging from 2.5 to 40 μM. The final DMSO concentration in culture medium did not exceed 0.1% (*v*/*v*) in any treatment, including vehicle controls. After 72 h, cells were fixed with 10% trichloroacetic acid (Sigma-Aldrich, cat. no. 27242) (50 μL/well) and stained with 0.4% SRB (Sigma-Aldrich, cat. no. 2S1403) dye (50 μL/well). After staining, unbound dye was removed by washing with 1% acetic acid, and plates were air-dried. The protein-bound sulforhodamine B (SRB) dye was solubilized with 100 μL per well of 10 mM Tris base (Sigma-Aldrich, cat. no. T8524; pH ~10.5). Absorbance was measured at 515 nm using a microplate reader (BMG Labtech, SuperStar Nano, Ortenberg, Germany) [25].

2.3. Molecular Modelling Study

Molecular docking simulations were performed using the crystal structure of murine COX-2 (PDB ID: 1CX2) complexed with celecoxib, retrieved from the Protein Data Bank [33]. The murine model was selected as a representative template for human COX-2 inhibition due to the high degree of structural homology and sequence identity (approx. 90%) between the two isoforms. Crucially, the residues defining the catalytic pocket and the secondary binding site—specifically Arg120, Tyr355, His90, and Val523—are strictly conserved across murine, ovine, and human species, ensuring that binding interactions predicted in the murine model are biologically relevant to the human enzyme [34].

Molecular docking simulations were performed to elucidate the binding orientations of compounds **6a–6d** within the cyclooxygenase active site. The X-ray crystal structure of Mus musculus COX-2 in complex with the selective inhibitor celecoxib was retrieved from the Protein Data Bank (PDB ID: 1CX2, resolution 3.0 Å) [35,36].

Protein and Ligand Preparation: For the docking protocol, only Chain A of the protein was retained. The co-crystallized ligand and water molecules were removed, and the protein structure was prepared using the DockPrep module within UCSF Chimera [37]. The 3D structures of compounds **6a**, **6b**, **6c**, **6d**, and the positive controls were generated using the Corina online service [38]. Subsequently, Gasteiger partial atomic charges were assigned to the ligands using OpenBabel [39].

Docking Parameters and Search Space: Docking was executed using AutoDock Vina v1.2.0 [40]. To accurately target the catalytic domain, the search space was defined by a cubic rid box centered on the geometric coordinates of the native ligand (celecoxib) within the CX2 structure. The grid center was set at X = 22.342, Y = 22.686, and Z = 17.373. The dimensions of the search volume were established at 27.5 × 27.8 × 29.4 Å, with a grid point spacing of 0.50 Å to ensure comprehensive coverage of the binding pocket. All other docking parameters were maintained at their default settings.

2.4. Statistical Analyses

All obtained results were expressed as the mean ± standard deviation (SD) from at least three independent experiments. For specific comparisons between two distinct groups where applicable, the unpaired t-test was employed. In all cases, a p-value < 0.05 was considered statistically significant. The IC_{50} values presented in Table 1 were determined by measuring the percentage inhibition across three or four concentrations (ranging from 0.01 to 30 μM). The resulting data points were fitted to a sigmoidal dose–response curve using non-linear regression analysis (log[inhibitor] vs. normalized response) in GraphPad Prism 9.0. This rigorous fitting model accounts for the high precision (three decimal places) of the reported inhibitory constants.

Table 1. IC_{50} values and the selectivity index of indole-acrylamide derivatives, in comparison with the positive control celecoxib.

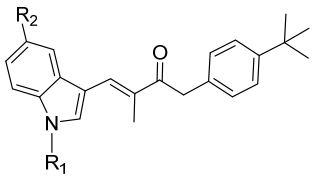

IC_{50} μM

Code	R1	R2	COX-1	COX-2	SI *	SI **
6a	CH_3	H	45.01 ± 1.27	0.128 ± 0.038	352	<0.01
6b	CH_3	Br	3.65 ± 0.27	0.218 ± 0.013	16	0.06
6c	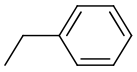	H	2.28 ± 0.24	0.215 ± 0.037	10.60	0.09
6d	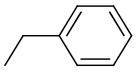	Br	<0.01	1.044 ± 0.040	<1	>100
Ketoprofen	-	-	0.039 ± 0.008	0.250 ± 0.011	0.156	6.4
Celecoxib	-	-	0.452 ± 0.095	0.0176 ± 0.007	25.68	0.04

* The COX-2 selectivity index (IC_{50} of COX-1/IC_{50} of COX-2). ** The COX-1 selectivity index (IC_{50} of COX-2/IC_{50} of COX-1), p value < 0.05.

3. Results

3.1. Chemistry

The synthetic methodology employed to synthesize the target compounds **6a–6d** is elucidated in Schemes 1 and 2. Methyl iodide or benzyl bromide was introduced into the solution of the starting compound (1H-indole-3-carbaldehyde) in anhydrous DMF in the

presence of sodium hydride to synthesize intermediates 1a-1d [41]. After that, the reaction was subsequently conducted for the synthesis of indol-acrylate ester derivatives (**2a**–**3b**), which is presented in Scheme 1. Then, by Wittig reaction (Scheme 1), the modified aldehyde with (carbethoxyethylidene) triphenylphosphorane, resulting in the formation of the ethyl ester [42], which was then hydrolyzed by using LiOH into (2E)-3-(1*H*-indol-3-yl)-2-methylprop-2-enoic acid derivatives (compound **4**–**5**), which were presented in Scheme 2 accordingly [26]. Finally, the final products are synthesized by a coupling process employing DMAP as an activating agent and EDCI as a coupling agent. After a 30 min reaction time, a 4-tert-butylaniline reactant was introduced to each reaction. Next, each reaction product was purified using column chromatography with different solvent systems (n-hexane and ethyl acetate) [43]. While the synthesis of **6a** and **6d** was previously described by Son et al. [43] in a different context, they were included in this study to serve as structural benchmarks for a systematic SAR analysis and to explore their previously uncharacterized role as selective COX-2 inhibitors in the context of hepatocellular carcinoma. Following purifications, the yields of all the final compounds fell within a 35–97% range. A wide range of spectrum data, including ^{1}H-NMR, ^{13}C-NMR, and HRMS, were used to analyze and verify all newly produced organic compounds.

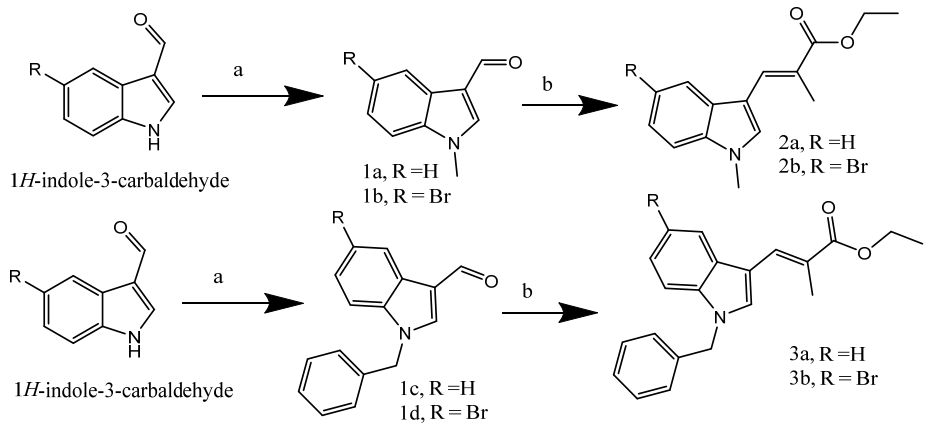

Scheme 1. Synthesis of indol-acrylate derivatives (**2a**–**3b**), (a) methyl iodide or benzyl bromide, NaH, DMF, inert gas, 5 °C for 3 h, (b) (Carbethoxyethylidene) triphenylphosphorane, DCM, room temperature.

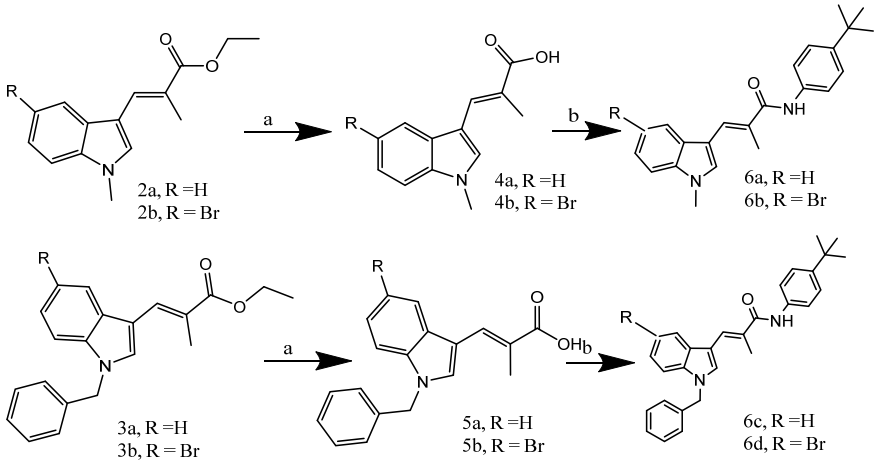

Scheme 2. Synthesis of indol-acrylamide derivatives (**6a**–**6d**). (a) Methanol/THF/water, LiOH, reflux. (b) 4-tert-butylaniline, EDC, DMAP, DCM, under inert gas, stirring 72 h.

3.2. Anti-Inflammatory (COX-1 and COX-2)

The in vitro analysis of COX enzyme inhibition activity evaluated the potential of the indole-acrylamide derivatives **6a–6d** to inhibit COX enzymes. The assessment was carried out using the COX-1 (ovine) and COX-2 (human) Inhibitor evaluation Assay Kit (Cayman Chemical Company, Ann Arbour, MI, USA) [29]. The observed inhibitory results at concentrations 30, 10, and 0.5 µM for these derivatives in comparison with the positive controls are presented in Figure 2. It was clear that the highest inhibitory percentage on the COX-2 enzyme at all concentrations was for compound **6a**, followed by compound **6c**. In contrast, compound **6d** showed significant activity against the COX-1 enzyme.

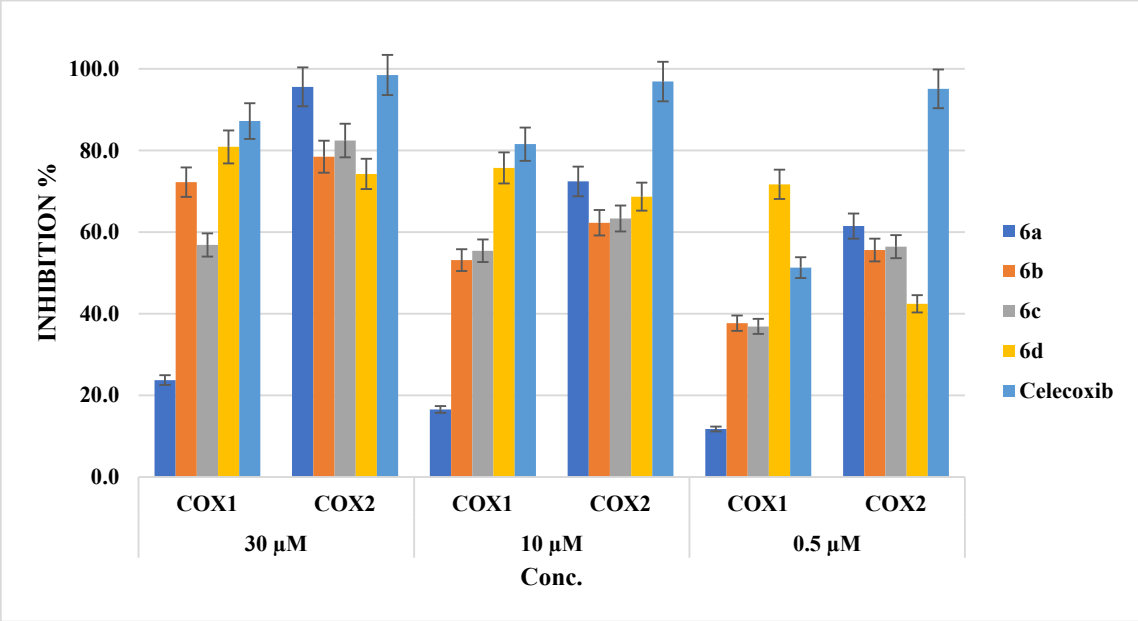

Figure 2. The inhibitory percentage on COX enzymes of indole-acrylamide derivatives compared with the positive control celecoxib.

According to the inhibitory percentage values, the most potent compound was compound **6a**, as presented in Table 1. The IC_{50} value of compound **6a** against COX-2 enzyme was 0.128 µM, and the selectivity ratio was 352. The presence of methyl at the indole cycle, like compounds **6a** and **6b**, was better for COX-2 inhibitory activities than the benzyl moiety, like compounds **6c** and **6d**. In contrast, the addition of the Br atom at the 6th position of the indole cycle increased the activities of the COX-1 enzyme.

3.3. Anticancer Activity

Cytotoxicity of the Indole-Acrylamide Derivatives in Cancer Cells

Elevated expression of cyclooxygenase (COX) enzymes has been firmly established in several forms of cancer, such as colon cancer, breast cancer, and melanoma [44,45]. Considering the possible correlation between COX enzymes and cancer, they are very convincing targets for the prevention and therapy of cancer. Aiming to clarify the mechanism of action processes involved in the novel indole-acrylamide derivatives and confirm their association with COX enzymes, the synthesized compounds were investigated in vitro for their anticancer properties against several cancer cell lines. The obtained results (Table 2) are expressed as IC_{50} values. All of the evaluated compounds showed significant antiproliferative activities against Huh7 with IC_{50} values in the range of 3.5–28.0 µM. Several works were conducted to find a relation between the COX inhibitors and antiproliferative effect on hepatocellular carcinoma cell lines [46,47]. A previous study provided evidence sup-

porting the notion that selective or, maybe more effectively, nonselective COX-2 inhibitors could have promising therapeutic benefits in hepatocellular carcinoma [48].

Table 2. IC_{50} values for the final synthesized compounds on cancer and normal cell lines.

	IC_{50} μM				
Cell Lines	**6a**	**6b**	**6c**	**6d**	**+ve Control**
Huh7	28.0 ± 1.9	11.6 ± 0.6	**4.7 ± 0.3**	**3.5 ± 0.6**	4.3 ± 0.5 [a]
MCF-7	15.4 ± 1.2	7.9 ± 0.3	6.0 ± 0.2	**3.5 ± 0.7**	14.6 ± 0.7 [a]
HCT116	17.4 ± 0.1	13.0 ± 0.3	6.6 ± 0.4	**4.5 ± 0.4**	10.8 ± 0.6 [a]
HepG2	NI	NI	8.0 ± 0.6	9.6 ± 0.6	3.2 ± 0.8 [a]
Mahlavu	NI	NI	7.5 ± 0.3	8.4 ± 1.2	7.5 ± 0.6 [a]
SNU475	NI	NI	4.2 ± 1.0	7.5 ± 0.1	5.2 ± 0.5 [a]
CaCo-2	NI	12.5 ± 1.1	NI	67.97 ± 0.8	6.68 ± 1.1 [b]
HeLa	146.4 ± 1.6	16.2 ± 0.4	NI	56.25 ± 0.2	1.33 ± 0.7 [b]
B16F1	**7.718 ± 0.5**	**4.748 ± 0.4**	10.699 ± 1.5	22.48 ± 2.4	82.45 ± 1.2 [b]
Hep3B	NI	71.79 ± 1.18	NI	74.09 ± 2.2	2.5 ± 0.8[a]
Hek293t	15.388 ± 1.67	59.44 ± 2.0	142.57 ± 1.3	14.93 ± 0.2	6.54 ± 1.0 [b]
SI	120.22	141.19	402.74	14.36	-

NI means no inhibition; SI: Selectivity index between CC_{50} of Hek293t and IC_{50} of COX2; +ve control: [a] Sorafenib & [b] 5-fluorouracil.

Interestingly, compound **6d** displayed potent antiproliferative effects (IC_{50} = 3.5, 4.5 μM in Huh7 and MCF-7, respectively) despite possessing the most moderate COX-2 inhibitory activity (IC_{50} = 1.04 μM) in the series. This suggests that the biological efficacy of **6d** may not be solely dependent on COX-2 affinity. Rather, its potency likely stems from a combination of favorable lipophilicity, which enhances cellular uptake, and potential polypharmacology. Indole derivatives are well-documented to engage multiple oncogenic pathways; therefore, **6d** likely exerts a synergistic effect where moderate COX-2 inhibition works in concert with secondary molecular targets to drive apoptosis.

Moreover, COX-1 selective inhibitors [49] or COX-2 selective inhibitors [50] showed anticancer activities against MCF-7 cancer cell lines, as well as compound **6d** (COX-1 selective) exhibited a significant MCF-7 antiproliferative effect with IC_{50} value of 3.5 μM and compounds **6a** and **6b** (COX-2 selective) showed significant anticancer activities on the cell lines with IC_{50} values of 15.4 and 7.9 μM respectively. Overexpression of the COX-2 enzyme in melanoma cancer was explored in many works, which could make COX-2 inhibitors possible candidates for melanoma cancer lead compounds [51,52]. According to our results, the COX-2 selective inhibitors compounds **6a** and **6b** were the most potent agents against melanoma cancer cell lines (B16F1) with IC_{50} values of 7.71 and 4.75 μM, respectively. These findings collectively position these agents as promising COX inhibitors and anticancer agents, underscored by their potent anti-proliferative effects and favorable selectivity profile.

To evaluate the safety profile and therapeutic window of the synthesized indole-acrylamide derivatives, the Selectivity Index (SI) was determined by comparing the IC_{50} values against the non-cancerous HEK293T cell line with the IC_{50} values against the targeted COX-2 enzyme and various cancer cell lines in Table 2. Notably, all compounds demonstrated a significant safety margin between enzymatic inhibition and general cellular toxicity. Compound **6c** emerged as the most promising lead in terms of safety, exhibiting an enzymatic SI of 402.74 (HEK293T CC_{50}/COX-2 IC_{50}), indicating that the concentration required to inhibit the target enzyme is several hundred times lower than the concentration inducing toxicity in normal kidney cells. Furthermore, the cellular SI for **6c** reached as high as 33.95 in SNU475 liver cancer cells. This superior selectivity, particularly when

compared to the positive control, which often displayed SI values below 1.0, underscores the potential of this scaffold to target cancerous phenotypes through a COX-2-mediated mechanism while minimizing off-target cytotoxicity to healthy human tissues.

While various indole-based derivatives have been explored for their anti-inflammatory properties [53], the current work introduces a uniquely optimized indole-acrylamide series specifically engineered for high-affinity COX-2 targeting in a cancer context. The novelty of this design lies in the strategic placement of the tert-butylphenyl substituent to interact with the COX-2-specific residues, an optimization strategy that differentiates this series from previous hybrids by achieving a superior selectivity index (SI > 350) and nanomolar potency.

The structural evolution of our current indole–acrylamide series was informed by a critical analysis of our previous lead compounds. Specifically, the indole–isoxazole derivative St.2 (Figure 1) had demonstrated potent cytotoxicity, IC_{50} 0.67 μM against MCF-7 cells. but exhibited relatively weak COX-2 inhibition (61% at 25 μM) [24], suggesting a lack of mechanistic synchronization. Subsequently, our work on isoxazole-carboxamides containing a tert-butylphenyl moiety (St.4, Figure 1) revealed a promising dual-effect profile, with IC_{50} values of 3.22 μg/mL against the COX-2 enzyme and potent antiproliferative activity against Hep3B (IC_{50} = 2.77 μg/mL) and MCF-7 (IC_{50} = 9.31 μg/mL) [27]. According to these findings, we strategically designed the current indole–acrylamide hybrids (**6a**–**6d**) to merge the high COX-affinity of the indole scaffold—a hallmark of classical NSAIDs—with the potent antiproliferative effect of the tert-butylphenyl carboxamide moiety.

This rational hybridization strategy was intended to "re-align" the enzymatic affinity with cellular potency, a goal that was successfully realized in the current work study. The breakthrough in this series is best shown by compound **6a**, which achieved a significant increase in lead potency with a COX-2 IC_{50} of 128 nM. This represents a nearly 200 times enhancement in enzymatic affinity compared to the inhibition levels of the earlier St.2. While these xenobiotics likely possess possible multi-targeted effects, the high affinity for COX-2 has now appeared as a more central and defining component of their biological profile. Furthermore, the shift from nanomolar enzymatic inhibition to micromolar cellular cytotoxicity for the **6a**–**6d** series aligns with well-known rules of drug–target interactions. This potency gap is typically attributed to the physiological barriers the compound must overcome, including cell membrane permeability, intracellular distribution, and non-specific binding to serum proteins.

Although our findings suggest a link between COX-2 inhibition and antiproliferative activity—most notably for the highly selective compound **6a**—this relationship cannot yet be considered conclusive. Additional downstream studies are needed to confirm whether the observed effects are truly COX-2 dependent. The cytotoxic response is likely driven by multiple contributing factors, with COX-2 inhibition playing a role through the reduction of pro-survival prostaglandin signaling. Future work, including PGE_2 rescue experiments and COX-2 gene silencing using siRNA, will be important to clearly separate COX-mediated activity from any secondary cytotoxic effects associated with the indole-acrylamide scaffold.

3.4. Molecular Modelling

Molecular docking was applied as a supplementary in silico method to support the results of the in vitro screening assays. COX enzymes play a major role in modulating cell proliferation and growth signaling pathways. Inhibition of these enzymes has proven effective as a therapeutic strategy for many types of malignancies [54]. Docking simulations were carried out for the entire compound series (**6a**–**6d**) to improve the robustness of the

experimental findings. The docking protocol was validated by re-docking celecoxib, which has achieved an RMSD of 0.01 Å, indicating an excellent predictive performance.

All synthesized indole–acrylamide hybrids showed appropriate binding interactions within the COX-2 active site (PDB ID: 1CX2). This provides a structural basis linking enzyme inhibition and the cellular antiproliferative activity discussed earlier. Specifically, the most selective compounds, **6a** and **6b**, clearly showed binding affinities of −8.392 and −8.195 kcal/mol, respectively. These findings are consistent with the discussed structure–activity relationship studies, indicating that the tert-butylphenyl moiety in the indole scaffold enhances the target-directed performance of this series.

An analysis of the predicted binding features indicates that the compound's potent enzymatic activity is associated with binding interactions similar to those of approved COX-2 inhibitors (Table 3). It forms a hydrogen bond with ARG120 at 3.18 Å and hydrophobic interactions with HIS90 and ARG120. These interactions are similar to those formed by celecoxib, which binds to ARG120 and HIS90 in the COX-2 pocket. In contrast, celecoxib exhibits broader binding interactions with 11 contacts and a stronger binding affinity (−10.969 kcal/mol). Compound **6a** forms seven binding interactions, supporting its strong inhibitory effect. Moreover, the binding mode of **6a** was highly reproducible in both AutoDock Vina and Chimera docking analyses.

Table 3. In silico docking analysis data of compounds **6a–6d** and celecoxib in the COX-2 pockets.

Ligand	COX	Binding Affinity (kcal/mol)	H-Interaction	Length in Å	Hydrophobic and Other Interactions	Length in Å
6a	COX-2	−8.392	ARG120	3.18	HIS90 ARG120 [5]	2.63 2.46–3.20
6b	COX-2	−8.195	-	-	ARG120 [2] HIS90 [2] ILE112 [5]	2.60–2.73 2.55–2.79 3.51
6c	COX-2	−8.255	-	-	ARG120 [5] HIS90 [3] ILE112 [4] LEU472 [2]	2.55–3.45 2.01–3.24 1.97–3.20 2.88–3.14
6d	COX-2	−7.964	-	-	HIS90 [2] ALA516 [2] SER353	2.97–3.68 2.65–3.01 2.39
Celecoxib	COX-2	−10.969	SER353 ARG513	2.11 2.37	HIS90 [3] TYR355 [3] VAL523 TRP387 ARG120	1.19–3.04 2.20–2.99 2.82 2.67 2.20

The [2], [3], [4], [5] numbers on the amino acids are related to the count of interactions.

Docking results for the remaining compounds support the structure–activity relationship studies of the entire series. Compound **6c**, which has the highest selectivity in cell-based assays, showed the strongest binding interaction −8.255 kcal/mol, and slo showed to be involved in binding with key residues, such as ARG120, HIS90, ILE112, and LEU472. Similarly, compound **6d**, which exhibits moderate enzymatic inhibition, showed a binding affinity of −7.964 kcal/mol via interactions with HIS90, ALA516, and SER353. Overall, the docking results exhibit a significant correlation with the observed biological activities, which confirms that a specific interaction with the COX-2 active site is a characteristic feature of the pharmacological profile of this indole–acrylamide series.

The molecular modeling test results provide insights into the structural features underlying the compounds' observed pharmacological behavior. Based on the calculated RMSD values, the predicted binding forces for compound **6a** were highly consistent with both AutoDock Vina and Chimera docking platforms. Visual inspection of the docking poses further emphasizes a clear correlation between the number of stabilizing molecular interactions and the measured enzymatic activity.

As shown in Figure 3A, compound **6a** formed seven defined interactions within the COX-2 active site. In contrast, celecoxib forms eleven contacts (Figure 3E), which explains its superior binding affinity. On the other hand, compound **6d** showed reduced binding, with only five contacts within the binding pocket (Figure 3D). This reduced number of interactions—and the associated moderate enzymatic inhibition—can be attributed to the orientation of its benzyl moiety, which was too far from the key ARG120 residue to allow effective engagement.

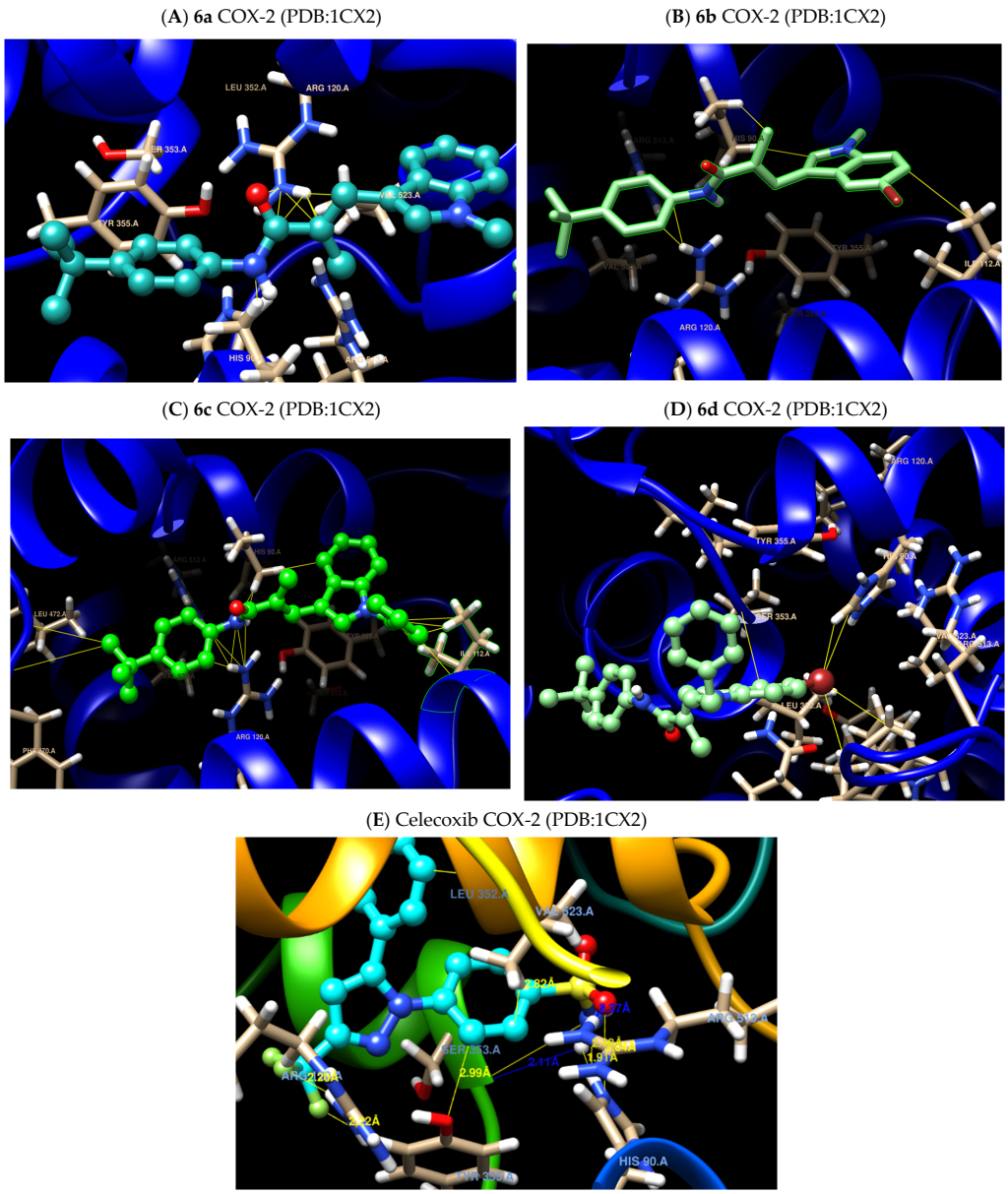

Figure 3. Molecular docking simulations within the COX-2 (PDB: 1CX2) binding pocket. (**A**) Compound **6a** demonstrates hydrogen bonding with ARG120 and hydrophobic interactions with HIS90. (**B**) Compound **6b** illustrates interactions with ARG120, HIS90, and ILE112. (**C**) Compound **6c** reveals an interaction network involving ARG120, HIS90, ILE112, and LEU472. (**D**) Compound **6d**

showing binding contacts with HIS90, ALA516, and SER353. (**E**) The positive control celecoxib depicts its established binding orientation with residues such as SER353, ARG513, HIS90, TYR355, VAL523, TRP387, and ARG120.

Interestingly, compound **6d** exhibited the highest selectivity for the COX-1 isoform, a finding that was explained by molecular docking results. In contrast to the potent COX-2 inhibitor **6a**, compound **6d** did not form the key hydrogen bond interaction with ARG120. Instead, it formed an interaction with other residues such as ALA516 and SER353.

Although systemic COX-1 inhibition is known to cause gastrointestinal and cardiovascular adverse effects, recent research has shown that selective COX-1 inhibitors have therapeutic benefits in certain cancers, including ovarian and specific colorectal malignancies, in which COX-1 is overexpressed [55]. Despite the COX-1 affinity of compound **6d**, it still maintains a safety margin, as reflected by a Selectivity Index (SI) of 4.27 in Huh7 cells relative to normal HEK293T cells. These findings suggest that the indole–acrylamide framework of **6d** may be a promising target for treating COX-1-dependent tumors, providing significant antiproliferative effects while maintaining a safety profile that is more manageable than that of conventional non-selective treatments, NSAIDs.

4. Conclusions

In summary, this research examined the design, synthesis, and biological evaluation of a new series of indole–acrylamide analogues as potent and selective COX-2 inhibitors. Among the tested series, compound **6a** is a promising lead, exhibiting nanomolar enzymatic inhibitory activity and high COX-2 selectivity. The results were supported by molecular docking studies against the COX-2 isoform. Although the binding scores were lower than those of the reference celecoxib, the results still provided a clear structural explanation for the observed selectivity. In particular, the indole–acrylamide scaffold was shown to effectively engage the COX-2–specific side pocket.

The tested compounds exhibited a wide range of anticancer activity across eleven cancer cell lines, with high potency against hepatocellular carcinoma, breast cancer, and melanoma models. Compounds **6a** and **6c** were the most selective inhibitors of COX-2; the potent COX-1 inhibitor compound **6d** showed anticancer activity against MCF-7 and Huh7 cells, suggesting that COX-1 may also be a target for certain tumors. The high Selectivity Indices (SI) observed between normal HEK293T cells and cancer models, as summarized in Table 2, indicate a robust safety margin and high therapeutic activity for this scaffold. Given these encouraging in vitro outcomes, this remains an exploratory study. Future investigations will expand the biological context through PGE2 rescue assays, apoptosis-induction studies, and cell-cycle analysis to definitively establish the causal link between COX inhibition and cytotoxicity. These derivatives represent a viable starting point for lead optimization and warrant further in vivo investigation to evaluate their pharmacokinetic properties.

Supplementary Materials: The following supporting information can be downloaded at: https://www.mdpi.com/article/10.3390/jox16020047/s1, Figure S1. (a) NMR spectrum of **6a**; (b): HRMS spectrum of **6a**; Figure S2. (a): NMR spectrum of **6b**; (b): HRMS spectrum of **6b**; Figure S3. (a): NMR spectrum of **6c**; (b): HRMS spectrum of **6c**; Figure S4. (a): NMR spectrum of **6d**; (b): HRMS spectrum of **6d**.

Author Contributions: Conceptualization, S.N.B. and M.H.; methodology, S.N.B. and M.H.; validation, B.M., D.C.K. and M.A.; formal analysis, B.M., D.C.K. and M.A.; investigation, B.M., D.C.K. and M.A.; resources, S.N.B. and M.H.; data curation, S.N.B. and M.H.; writing—original draft preparation, S.N.B., D.C.K. and M.H.; writing—review and editing, S.N.B. and M.H.; visualization, S.N.B.

and M.H.; supervision, S.N.B. and M.H.; project administration, S.N.B. and M.H. All authors have read and agreed to the published version of the manuscript.

Funding: This research was funded by the Scientific and Technological Research Council of Turkey (TUBITAK), grant number 'program 2209-A' to B.M.

Institutional Review Board Statement: Not applicable.

Informed Consent Statement: Not applicable.

Data Availability Statement: The original contributions presented in this study are included in the article/Supplementary Material. Further inquiries can be directed to the corresponding authors.

Acknowledgments: This work was supported by the Scientific and Technological Research Council of Turkey (TUBITAK) (program 2209-A) to Benay Mahmutoglu. The authors would like to thank Gazi University, An-Najah National University and Middle East Technical University, for their support of this work.

Conflicts of Interest: The authors declare no conflicts of interest.

Abbreviations

The following abbreviations are used in this manuscript:

COX	Cyclooxygenase enzyme
DMSO	Dimethyl sulfoxide
HRMS	High-resolution mass spectrometer
NMR	Nuclear magnetic resonance
M.P.	Melting points
IC_{50}	Half maximal inhibitory concentration
MCF7	Human breast cancer cell line
HCT116	colon cancer cell lines
HepG2	Liver cancer cell lines
HCC	Hepatocellular carcinoma
HeLa	cervical cancer cell lines
Conc.	Concentration
DMAP	Dimethylaminopyridine
DMF	Dimethylformamide
EDC	1-Ethyl-3-(3-dimethylaminopropyl) carbodiimide
LiOH	Lithium hydroxide
TLC	Thin-layer chromatography

References

1. Khan, H.Y.; Parveen, S.; Yousuf, I.; Tabassum, S.; Arjmand, F. Metal complexes of NSAIDs as potent anti-tumor chemotherapeutics: Mechanistic insights into cytotoxic activity via multiple pathways primarily by inhibition of COX–1 and COX–2 enzymes. *Coord. Chem. Rev.* **2022**, *453*, 214316. [CrossRef]
2. Faura, G.G.; Wu, B.; Oyelere, A.K.; France, S. Synthetic methodology-enabled discovery of a tunable indole template for COX-1 inhibition and anti-cancer activity. *Bioorg. Med. Chem.* **2022**, *57*, 116633. [CrossRef] [PubMed]
3. Zhong, B.; Cai, X.; Chennamaneni, S.; Yi, X.; Liu, L.; Pink, J.J.; Dowlati, A.; Xu, Y.; Zhou, A.; Su, B. From COX-2 inhibitor nimesulide to potent anti-cancer agent: Synthesis, in vitro, in vivo and pharmacokinetic evaluation. *Eur. J. Med. Chem.* **2012**, *47*, 432–444. [CrossRef] [PubMed]
4. Abdelgawad, M.A.; Bakr, R.B.; Omar, H.A. Design, synthesis and biological evaluation of some novel benzothiazole/benzoxazole and/or benzimidazole derivatives incorporating a pyrazole scaffold as antiproliferative agents. *Bioorg. Chem.* **2017**, *74*, 82–90. [CrossRef] [PubMed]
5. Nyegaard, S.; Novakovic, V.A.; Rasmussen, J.T.; Gilbert, G.E. Lactadherin inhibits secretory phospholipase A_2 activity on pre-apoptotic leukemia cells. *PLoS ONE* **2013**, *8*, e77143. [CrossRef]
6. Cao, Y.; Prescott, S.M. Many actions of cyclooxygenase-2 in cellular dynamics and in cancer. *J. Cell. Physiol.* **2002**, *190*, 279–286. [CrossRef]

7. Secchiero, P.; Barbarotto, E.; Gonelli, A.; Tiribelli, M.; Zerbinati, C.; Celeghini, C.; Agostinelli, C.; Pileri, S.A.; Zauli, G. Potential pathogenetic implications of cyclooxygenase-2 overexpression in B chronic lymphoid leukemia cells. *Am. J. Pathol.* **2005**, *167*, 1599–1607. [CrossRef]
8. Sivula, A.; Talvensaari-Mattila, A.; Lundin, J.; Joensuu, H.; Haglund, C.; Ristimäki, A.; Turpeenniemi-Hujanen, T. Association of cyclooxygenase-2 and matrix metalloproteinase-2 expression in human breast cancer. *Breast Cancer Res. Treat.* **2005**, *89*, 215–220. [CrossRef]
9. Xu, H.-B.; Shen, F.-M.; Lv, Q.-Z. Celecoxib enhanced the cytotoxic effect of cisplatin in chemo-resistant gastric cancer xenograft mouse models through a cyclooxygenase-2-dependent manner. *Eur. J. Pharmacol.* **2016**, *776*, 1–8. [CrossRef]
10. Kassab, A.E. Recent advances in targeting COX-2 for cancer therapy: A review. *RSC Med. Chem.* **2025**, *16*, 2974–3002. [CrossRef]
11. Kuang, B.; Yang, K.; Zhong, X.; Tan, Y.; Zhou, Y.; Ye, J. Celecoxib in oncology: Targeting the COX-2/PGE_2 axis to reprogram the tumor immune microenvironment and enhance multimodal therapy. *Front. Pharmacol.* **2025**, *16*, 1691392. [CrossRef]
12. Galal, S.A.; Khairat, S.H.; Ragab, F.A.; Abdelsamie, A.S.; Ali, M.M.; Soliman, S.M.; Mortier, J.; Wolber, G.; El Diwani, H.I. Design, synthesis and molecular docking study of novel quinoxalin-2 (1H)-ones as anti-tumor active agents with inhibition of tyrosine kinase receptor and studying their cyclooxygenase-2 activity. *Eur. J. Med. Chem.* **2014**, *86*, 122–132. [CrossRef]
13. Arun, B.; Goss, P. The role of COX-2 inhibition in breast cancer treatment and prevention. *Semin. Oncol.* **2004**, *31*, 22–29. [CrossRef] [PubMed]
14. Miller, K.D.; Siegel, R.L.; Lin, C.C.; Mariotto, A.B.; Kramer, J.L.; Rowland, J.H.; Stein, K.D.; Alteri, R.; Jemal, A. Cancer treatment and survivorship statistics, 2016. *CA Cancer J. Clin.* **2016**, *66*, 271–289. [CrossRef] [PubMed]
15. Ferrandez, A.; Prescott, S.; Burt, R. COX-2 and colorectal cancer. *Curr. Pharm. Des.* **2003**, *9*, 2229–2251. [CrossRef] [PubMed]
16. Wang, D.; DuBois, R.N. The role of COX-2 in intestinal inflammation and colorectal cancer. *Oncogene* **2010**, *29*, 781–788. [CrossRef]
17. Bhat, M.A.; Al-Omar, M.A.; Raish, M.; Ansari, M.A.; Abuelizz, H.A.; Bakheit, A.H.; Naglah, A.M. Indole derivatives as cyclooxygenase inhibitors: Synthesis, biological evaluation and docking studies. *Molecules* **2018**, *23*, 1250. [CrossRef]
18. Hawash, M.; Ergun, S.G.; Kahraman, D.C.; Olgac, A.; Hamel, E.; Cetin-Atalay, R.; Baytas, S.N. Novel indole-pyrazole hybrids as potential tubulin-targeting agents; Synthesis, antiproliferative evaluation, and molecular modeling studies. *J. Mol. Struct.* **2023**, *1285*, 135477. [CrossRef]
19. Misra, S.K.; Pathak, D.; Pathak, K. Anticancer potential of indole derivatives: An update. *Phys. Sci. Rev.* **2023**, *8*, 1545–1569. [CrossRef]
20. Sever, B.; Altıntop, M.D.; Özdemir, A.; Akalın Çiftçi, G.; Ellakwa, D.E.; Tateishi, H.; Radwan, M.O.; Ibrahim, M.A.; Otsuka, M.; Fujita, M. In vitro and in silico evaluation of anticancer activity of new indole-based 1, 3, 4-oxadiazoles as EGFR and COX-2 inhibitors. *Molecules* **2020**, *25*, 5190. [CrossRef]
21. Mohsin, N.U.A.; Aslam, S.; Ahmad, M.; Irfan, M.; Al-Hussain, S.A.; Zaki, M.E. Cyclooxygenase-2 (COX-2) as a target of anticancer agents: A review of novel synthesized scaffolds having anticancer and COX-2 inhibitory potentialities. *Pharmaceuticals* **2022**, *15*, 1471. [CrossRef]
22. Niho, N.; Kitamura, T.; Takahashi, M.; Mutoh, M.; Sato, H.; Matsuura, M.; Sugimura, T.; Wakabayashi, K. Suppression of azoxymethane-induced colon cancer development in rats by a cyclooxygenase-1 selective inhibitor, mofezolac. *Cancer Sci.* **2006**, *97*, 1011–1014. [CrossRef] [PubMed]
23. Penthala, N.R.; Ponugoti, P.R.; Kasam, V.; Crooks, P.A. 5-((1-Aroyl-1H-indol-3-yl) methylene)-2-thioxodihydropyrimidine-4, 6 (1H, 5H)-diones as potential anticancer agents with anti-inflammatory properties. *Bioorg. Med. Chem. Lett.* **2013**, *23*, 1442–1446. [CrossRef] [PubMed]
24. Kumari, P.; Mishra, V.S.; Narayana, C.; Khanna, A.; Chakrabarty, A.; Sagar, R. Design and efficient synthesis of pyrazoline and isoxazole bridged indole C-glycoside hybrids as potential anticancer agents. *Sci. Rep.* **2020**, *10*, 6660. [CrossRef] [PubMed]
25. Hawash, M.; Kahraman, D.C.; Cetin-Atalay, R.; Baytas, S.N. Induction of Apoptosis in Hepatocellular Carcinoma Cell Lines by Novel Indolylacrylamide Derivatives: Synthesis and Biological Evaluation. *Chem. Biodivers.* **2021**, *18*, e2001037. [CrossRef]
26. Hawash, M.; Kahraman, D.C.; Ergun, S.G.; Cetin-Atalay, R.; Baytas, S.N. Synthesis of novel indole-isoxazole hybrids and evaluation of their cytotoxic activities on hepatocellular carcinoma cell lines. *BMC Chem.* **2021**, *15*, 66. [CrossRef]
27. Hawash, M.; Jaradat, N.; Abualhasan, M.; Qneibi, M.; Rifai, H.; Saqfelhait, T.; Shqirat, Y.; Nazal, A.; Omarya, S.; Ibrahim, T.; et al. Evaluation of cytotoxic, COX inhibitory, and antimicrobial activities of novel isoxazole-carboxamide derivatives. *Lett. Drug Des. Discov.* **2022**, *20*, 1994–2002. [CrossRef]
28. Hawash, M.; Jaradat, N.; Sabobeh, R.; Abualhasan, M.; Qaoud, M.T. New Thiazole Carboxamide Derivatives as COX Inhibitors: Design, Synthesis, Anticancer Screening, In Silico Molecular Docking, and ADME Profile Studies. *ACS Omega* **2023**, *8*, 29512–29526. [CrossRef]
29. Drazen, J.M. COX-2 inhibitors—a lesson in unexpected problems. *N. Engl. J. Med.* **2005**, *352*, 1131–1132. [CrossRef]
30. Oefinger, P.E.; Bronson, D.L.; Dreesman, G.R. Induction of hepatitis B surface antigen in human hepatoma-derived cell lines. *J. Gen. Virol.* **1981**, *53*, 105–113. [CrossRef]

31. Hawash, M.; Qaoud, M.T.; Jaradat, N.; Abdallah, S.; Issa, S.; Adnan, N.; Hoshya, M.; Sobuh, S.; Hawash, Z. Anticancer Activity of Thiophene Carboxamide Derivatives as CA-4 Biomimetics: Synthesis, Biological Potency, 3D Spheroid Model, and Molecular Dynamics Simulation. *Biomimetics* **2022**, *7*, 247. [CrossRef] [PubMed]
32. Shi, M.; Ho, K.; Keating, A.; Shoichet, M.S. Doxorubicin-conjugated immuno-nanoparticles for intracellular anticancer drug delivery. *Adv. Funct. Mater.* **2009**, *19*, 1689–1696. [CrossRef]
33. Samineni, R.; Samathoti, P.; Gouru, S.A.; Khan, A.; Sp, P.P.; Manda, K. In-silico investigation and development of cyclooxygenase-2 (1CX2) selective inhibition as a possible anti-inflammatory activity. *Biomed. Pharmacol. J.* **2024**, *17*, 1769–1783. [CrossRef]
34. Araújo, P.H.; Ramos, R.S.; da Cruz, J.N.; Silva, S.G.; Ferreira, E.F.; de Lima, L.R.; Macêdo, W.J.; Espejo-Román, J.M.; Campos, J.M.; Santos, C.B. Identification of potential COX-2 inhibitors for the treatment of inflammatory diseases using molecular modeling approaches. *Molecules* **2020**, *25*, 4183. [CrossRef]
35. Berman, H.M.; Battistuz, T.; Bhat, T.N.; Bluhm, W.F.; Bourne, P.E.; Burkhardt, K.; Feng, Z.; Gilliland, G.L.; Iype, L.; Jain, S. The protein data bank. *Acta Crystallogr. Sect. D Biol. Crystallogr.* **2002**, *58*, 899–907. [CrossRef]
36. Cingolani, G.; Panella, A.; Perrone, M.G.; Vitale, P.; Di Mauro, G.; Fortuna, C.G.; Armen, R.S.; Ferorelli, S.; Smith, W.L.; Scilimati, A. Structural basis for selective inhibition of Cyclooxygenase-1 (COX-1) by diarylisoxazoles mofezolac and 3-(5-chlorofuran-2-yl)-5-methyl-4-phenylisoxazole (P6). *Eur. J. Med. Chem.* **2017**, *138*, 661–668. [CrossRef]
37. Pettersen, E.F.; Goddard, T.D.; Huang, C.C.; Couch, G.S.; Greenblatt, D.M.; Meng, E.C.; Ferrin, T.E. UCSF Chimera—A visualization system for exploratory research and analysis. *J. Comput. Chem.* **2004**, *25*, 1605–1612. [CrossRef]
38. Sadowski, J.; Gasteiger, J.; Klebe, G. Comparison of automatic three-dimensional model builders using 639 X-ray structures. *J. Chem. Inf. Comput. Sci.* **1994**, *34*, 1000–1008. [CrossRef]
39. O'Boyle, N.M.; Banck, M.; James, C.A.; Morley, C.; Vandermeersch, T.; Hutchison, G.R. Open Babel: An open chemical toolbox. *J. Cheminform.* **2011**, *3*, 33. [CrossRef]
40. Trott, O.; Olson, A.J. AutoDock Vina: Improving the speed and accuracy of docking with a new scoring function, efficient optimization, and multithreading. *J. Comput. Chem.* **2010**, *31*, 455–461. [CrossRef]
41. Akhlaghi, M.F.; Amidi, S.; Esfahanizadeh, M.; Daeihamed, M.; Kobarfard, F. Synthesis of N-arylmethyl substituted indole derivatives as new antiplatelet aggregation agents. *Iran. J. Pharm. Res. IJPR* **2014**, *13*, 35.
42. Jin, G.; Lee, S.; Choi, M.; Son, S.; Kim, G.-W.; Oh, J.-W.; Lee, C.; Lee, K. Chemical genetics-based discovery of indole derivatives as HCV NS5B polymerase inhibitors. *Eur. J. Med. Chem.* **2014**, *75*, 413–425. [CrossRef] [PubMed]
43. Son, S.; Kim, D.; Lee, S.; Jin, G.; Park, J.A.; Han, H.K.; Lee, K.; Lee, C. Synthesis and Structure–Activity Relationship of Novel Indole Acrylamide Derivatives as HCV Replication Inhibitors. *Bull. Korean Chem. Soc.* **2015**, *36*, 88–98. [CrossRef]
44. Abdelazeem, A.H.; Gouda, A.M.; Omar, H.A.; Tolba, M.F. Design, synthesis and biological evaluation of novel diphenylthiazole-based cyclooxygenase inhibitors as potential anticancer agents. *Bioorg. Chem.* **2014**, *57*, 132–141. [CrossRef]
45. Kast, R. Melanoma inhibition by cyclooxygenase inhibitors: Role of interleukin-6 suppression, a putative mechanism of action, and clinical implications. *Med. Oncol.* **2007**, *24*, 1–6. [CrossRef]
46. Afzal, M.; Bhardwaj, D.; Khan, R.; Kazmi, I.; Saleem, S.; Al-Abbasi, F.; Anwar, F. Antineoplastic influence of nimesulide in chemically induced hepatocellular carcinoma by inhibition of DNA synthesis. *Inflammopharmacology* **2019**, *27*, 89–98. [CrossRef]
47. Narożna, M.; Krajka-Kuźniak, V.; Bednarczyk-Cwynar, B.; Baer-Dubowska, W. Unlocking the potential: Novel NSAIDs hybrids unleash chemopreventive power toward liver cancer cells through Nrf2, NF-κB, and MAPK signaling pathways. *Molecules* **2023**, *28*, 5759. [CrossRef]
48. Foderà, D.; D'ALESSANDRO, N.; Cusimano, A.; Poma, P.; Notarbartolo, M.; Lampiasi, N.; Montalto, G.; Cervello, M. Induction of apoptosis and inhibition of cell growth in human hepatocellular carcinoma cells by COX-2 inhibitors. *Ann. N. Y. Acad. Sci.* **2004**, *1028*, 440–449. [CrossRef]
49. Jeong, H.-S.; Kim, J.-H.; Choi, H.Y.; Lee, E.-R.; Cho, S.-G. Induction of cell growth arrest and apoptotic cell death in human breast cancer MCF-7 cells by the COX-1 inhibitor FR122047. *Oncol. Rep.* **2010**, *24*, 351–356. [CrossRef]
50. Yuan, L.; Jiang, R.; Yang, Y.; Ding, S.; Deng, H. 1, 25-Dihydroxyvitamin D3 inhibits growth of the breast cancer cell line MCF-7 and downregulates cytochrome P4501B1 through the COX-2/PGE2 pathway. *Oncol. Rep.* **2012**, *28*, 2131–2137. [CrossRef]
51. Tudor, D.V.; Bâldea, I.; Lupu, M.; Kacso, T.; Kutasi, E.; Hopârtean, A.; Stretea, R.; Filip, A.G. COX-2 as a potential biomarker and therapeutic target in melanoma. *Cancer Biol. Med.* **2020**, *17*, 20. [CrossRef]
52. Botti, G.; Fratangelo, F.; Cerrone, M.; Liguori, G.; Cantile, M.; Anniciello, A.M.; Scala, S.; D'Alterio, C.; Trimarco, C.; Ianaro, A. COX-2 expression positively correlates with PD-L1 expression in human melanoma cells. *J. Transl. Med.* **2017**, *15*, 46. [CrossRef]
53. Suliphuldevara Mathada, B.; Gunavanthrao Yernale, N.; Basha, J.N. The multi-pharmacological targeted role of indole and its derivatives: A review. *ChemistrySelect* **2023**, *8*, e202204181. [CrossRef]

54. Hawash, M.; Abdallah, S.; Abudayyak, M.; Melhem, Y.; Shamat, M.A.; Aghbar, M.; Çapan, I.; Abualhasan, M.; Kumar, A.; Kamiński, M. Exploration of isoxazole analogs: Synthesis, COX inhibition, anticancer screening, 3D multicellular tumor spheroids, and molecular modeling. *Eur. J. Med. Chem.* **2024**, *271*, 116397. [CrossRef]
55. Pannunzio, A.; Coluccia, M. Cyclooxygenase-1 (COX-1) and COX-1 inhibitors in cancer: A review of oncology and medicinal chemistry literature. *Pharmaceuticals* **2018**, *11*, 101. [CrossRef]